Experimental Mechanics (2022) 62:799–812
https://doi.org/10.1007/s11340-022-00829-7

RESEARCH PAPER

A Comparison of Conventional Gel Stiffness Characterization Techniques with Cavitation Rheology

Y. Ji[1] · A. M. Dagro[2] · G. Dorgant[1] · D. Starr[1] · J. W. Wilkerson[1]

Received: 10 December 2020 / Accepted: 12 February 2022 / Published online: 1 March 2022

Abstract

Background Interest in soft gels has arisen in recent years as they can be applied to many fields such as tissue engineering, food additives, and drug delivery. The importance of these technologies lies in the stiffness of applied materials and hence there is a strong need for determining the stiffness of gels precisely. Cavitation rheology, a novel experimental method, can measure the Young's modulus in any part of a soft material. However, compared with fully developed conventional techniques, cavitation rheology is not completely exploited and needs more in-depth research conducted.

Objective In this paper, four experimental approaches have been applied to determine the Young's modulus of an ultra-soft tri-block copolymer (PMMA-PnBA-PMMA): classic shear rheology, static indentation, cavitation rheology and low-velocity impact. Although there are plenty of examples of soft gel stiffness characterization in the open literature, this is the first time (to the knowledge of the authors), that cavitation rheology and the impact pinch-off experiment have been compared with the more traditional stiffness testing approaches of classic rheology and indentation. Furthermore, the relationship between gel's stiffness and the von Mises strain rate is investigated in the analysis.

Methods Benchmark data is obtained from a classic shear rheology experiment. A modification to the previous cavitation rheology analysis is made to improve the accuracy in predicting the Young's modulus and surface tension. The measurements of static indentation and dynamic low-velocity impact experiments are taken non-invasively by optical visualization. Gel samples with three concentrations are applied to all the experiments to investigate the feasibility of each method.

Results The comparison between different experiments indicates a slight strain-rate dependence in gel stiffness across various gel concentrations. Cavitation rheology is shown to have a clear correlation with high-strain rate tests, but not quasi-static ones.

Conclusions This paper has made some significant contributions in regards to broadening the knowledge of cavitation rheology. In addition, we provide an in-depth analysis of pragmatic stiffness measurement techniques and demonstrate their usefulness across various stiffness regimes in a soft polymeric gel with tunable mechanical properties.

Keywords Soft solids · Gel stiffness characterization · Mechanical properties of soft gels · Cavitation · Indentation · Impact

Introduction

Gels are characterized as a cross-linked system without flow in the steady state [1]. They behave like solids due to the feature of cross-linked networks within the liquid. Considering the fact that gels can be tailored for having similar mechanical properties as soft human tissues, they are suitable candidate materials in the fields of biomechanics and tissue engineering. Accurately measuring the mechanical properties of soft tissues is essential for understanding disease development [2–4], examining human mortality [5], and designing future biomaterials [6–8]. The stiffness, often quantified as Young's modulus, of human tissues can vary over an order of magnitude (e.g., from 460 *Pa* for liver [9] to 45 *kPa* for thyroid [10] measured at the lowest strain rate and lowest pre-strain under compression). Creating accurate, reproducible, and inexpensive tests to measure the mechanical properties of gels over a wide range of stiffness is an ongoing challenge. Conventional bulk mechanical tests such

✉ J. W. Wilkerson
wilkerson@tamu.edu

[1] Department of Mechanical Engineering, Texas A&M University, College Station, TX 77843, USA

[2] CCDC U.S. Army Research Laboratory, Aberdeen Proving Ground, Aberdeen, MD 21005, USA

as tensile and compression tests have been applied to determine the mechanical properties of soft materials, but they are not the optimal choice due to the difficulties of designing fixtures and gripping samples [11]. In addition, sophisticated characterization techniques like nano-indentation have complications with respect to surface detection, adhesion, and probe geometries [12]. Compared with these methods, cavitation rheology, indentation and low-velocity impact experiments are inherently simple and avoid some of the aforementioned complications.

Cavitation rheology, introduced by Zimberlin et al. [13], can measure the local Young's modulus in any part of a soft material. The principle of the method is to intentionally create a defect inside the material by inserting a needle and pressurize the defect by pumping air into it. This technique is also called needle-induced cavitation, which has been widely applied to material characterization [14–17]. In addition, recent experimental evidence indicates that traumatic brain injury (TBI) may be related to cavitation induced during sudden impacts [18–21].

The non-dimensional number which characterizes common phenomena such as the splash and cavity caused by the entry of a solid into a liquid is the Froude number, $Fr \sim U_0^2/gd$, where U_0 is the characteristic velocity at entry, g is the gravitation acceleration, and d is the characteristic length (e.g., the diameter of a spherical projectile) [22–25]. Previous ballistic experiments [26, 27] showed how a stiff triblock copolymer and a viscoelastic micellar fluid responded to high-velocity (100–500 *m/s*) and low-velocity (~ 2.4 *m/s*) impacts, respectively. Despite differences between ballistic experiments (impact velocities, projectile properties and test material properties), there exists a similar power-law relationship between the normalized initial penetration depth and the modified Froude number, *Fe*, which takes elasticity into account. The related analysis provides motivation in the development of our low-velocity impact experiment to investigate soft gels.

In this paper, the benchmark Young's moduli of three gel concentrations is first obtained from a classic shear rheology experiment. Then the results from cavitation rheology, static indentation and low-velocity impact are compared with the above data, taking into account the effects of gel cross-linker concentration. Throughout the paper, it is assumed that the gel specimens are isotropic and incompressible (Poisson's ratio $\nu = 0.5$). Therefore, the shear modulus μ_0 can be converted to the Young's modulus E by the equation $E = 2\mu_0(1 + \nu) = 3\mu_0$. The von Mises strain rate is calculated for each experiment. The relationship between stiffness of gel materials and strain rate is examined in the discussion part. Moreover, the detailed analysis of the discrepancy in the predicted Young's moduli using different methods is performed, and the limitations of each experiment are discussed.

Experimental Methodology

Material Preparation

A triblock copolymer poly-(methyl methacrylate)- poly (n-butyl acrylate)- poly (methyl methacrylate), commonly referred as PMMA-PnBA-PMMA, was used in all experiments. The copolymer samples whose PMMA end-block and PnBA mid-block are 8,900 *g/mol* and 53, 000 *g/mol* were kindly provided by Kuraray Co. Ltd. The properties of the thermoreversible gel are strongly dependent with temperature. When the temperature is increased over the critical micelle temperature, the endblock aggregates and a low-viscosity liquid is formed [28]. Below the critical micelle temperature, the spherical aggregates formed by self-assembly of end-blocks serve as cross-links, interconnected by mid-blocks, which results in a viscoelastic liquid. During the cooling process, the transition from liquid to solid can be observed. Previous experiments showed that the transition temperatures of 5% v/v and 10% v/v gels in 2-ethyl-1-hexanol were close to 34 °C [29] and 40 °C [30], respectively. As the system is cooled below the glass transition temperature, a strong elastic network with a long relaxation time is developed. In spite of the concentration and block length dependence, the glass transition temperature of the solvent-swollen endblock domains is proved to be between 23 °C and the critical micelle temperature of the solid gels [31]. The linear elastic properties which are characterized by the initial shear modulus are shown in this elastic regime [29].

To make the test material, copolymer samples were dissolved in 2-ethyl-1-hexanol at 80 °C. After mixing for two hours, the material was removed from the hot plate to cool down to 23 °C. Three concentrations of gels (4.69, 7.89 and 11.89 % v/v) were applied to our experiments.

Shear Rheology Experiment

Shear rheology experiments were performed using an Anton-Paar's MCR 302 Rheometer at 22 °C. Previous studies report that soft materials do not report different responses in experiments using parallel-plate versus cone-plate geometries [32]. A parallel-plate geometry (25 *mm* in diameter, 1 *mm* gap) was applied to all the experiments. Gel samples were loaded on the base plate of the rheometer in a liquid state (at 45 °C). Then they were cooled and equilibrated at 22 °C for 5 *min* before experiments to guarantee a firm adhesion between sample and fixture. Three different frequencies (1, 5 and 10 *Hz*) were employed in the strain-amplitude sweep experiment for gel samples. A frequency-sweep experiment was also conducted to investigate the relationship between gel's response and sweep frequency.

Cavitation Rheology Experiment

The cavitation rheology experiment introduced by Zimberlin et al. [13] was conducted to measure the Young's modulus of soft gels. It was performed by a customized apparatus shown in Fig. 1(a) at 23 °C. A syringe pump (NE1000 from New Era), a flat-ended needle and a pressure transducer (Omega PX409-005GUSBH, the maximum pressure shown was around 46 *kPa*) were connected by tubes and other fittings. Metal hub (nickel plated brass) needles (Hamilton) with different radii were inserted into the soft material to create cavities. The injection operation was carried out by raising a high-precision lab jack where the material was placed. The travel distance was fixed to be 10 *mm* for all the experiments. Four different needles (12, 20, 24, and 30 *GA*) were applied and two flow rates (2 *mL/min* and 10 *mL/min*) were set for the syringe pump, assuming that the difference between these two flow rates would not affect the measurement of critical pressure. The experimental raw data and plots could be obtained from the Digital Transducer Application. Meanwhile, the growth of the cavity was recorded by a high-speed camera (Edgertronic, SC2+, 1000 *fps*). The images were used to calculate the cavity radius and the expansion rate for each applied needle.

Static Indentation Experiment

The set-up of the indentation experiment is shown in Fig. 1(b). The gel sample height and the width of the square container were controlled much larger than the indentation depth in order to mitigate possible substrate effects and confining effects of container. Six different steel balls with smooth surfaces (diameters varied between 6.32 *mm* and 25.35 *mm*) were gently put on the gel surface. The solid steel indenters used for the 4.69% v/v gel made the indentation depth larger than the indenter's radius. Therefore, several hollow aluminum indenters were employed to this gel concentration. An image was captured from the front immediately after each indenter reached a steady state. An accurate pixel measurement was carried out afterwards by WebPlotDigitizer and the result could be converted to actual distance with reference to a paper ruler. Both indentation depth and contact diameter were obtained using this method. The contact diameter was determined by directly measuring the distance between two points where the local curvature showed an abrupt change (Fig. 1(b)).

Table 1 Material densities in the unit of kg/m^3 in the dynamic low-velocity impact experiment

Steel projectile 1	Steel projectile 2	Marble projectile	4.69% v/v gel	7.89% v/v gel	11.89% v/v gel
7.93	7.92	2.51	0.80	0.81	0.86

Dynamic Low-Velocity Impact Experiment

Two steel spherical projectiles (15.79 and 18.98 *mm* in diameter) were dropped from 0.5 *m* into three different gels (Fig. 1(c)). To minimize the influence caused by the density of the projectile and other parameters, the same experiment was performed later using a marble projectile (24.66 *mm* in diameter). The densities of projectiles and three different gels are included in Table 1. It was assumed that the surface of each projectile was smooth and no friction was generated. All the snapshots were obtained by the SC2+ high-speed camera from Edgertronic at a rate of 5000 *fps*. The impact velocity was considered as the velocity just before the projectile had a physical contact with the gel surface. Ten consecutive snapshots before the contact were collected for each experiment. Pixel measurements were taken for these snapshots and they were converted to actual distances. A linear trendline was applied to the discrete data points for each plot so that the velocity could be determined given the time interval. The measured impact velocities are comparable to the theoretical values calculated from $\sqrt{2gH}$, where g is the acceleration of gravity

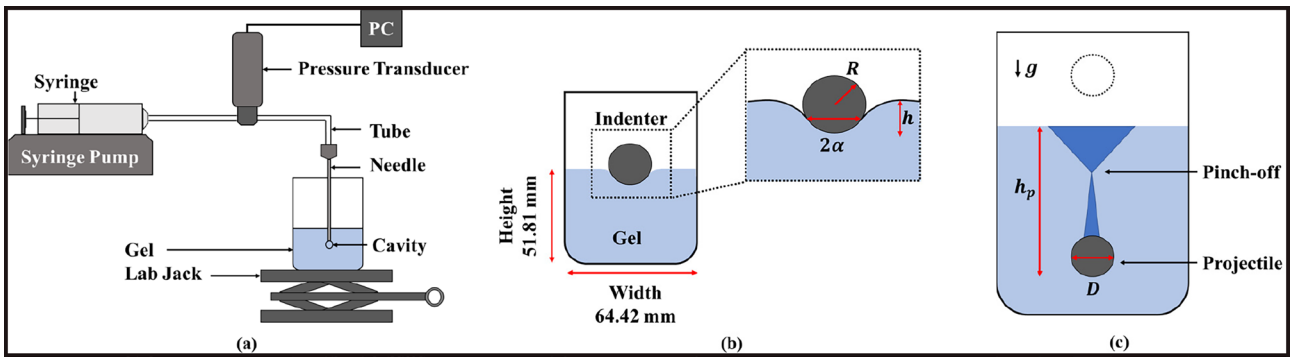

Fig. 1 The schematics of (**a**) cavitation rheology experiment, (**b**) static indentation experiment, and (**c**) dynamic low-velocity impact experiment. The variables R, α and h in (**b**) represent the radius of the indenter, contact radius and indentation depth, respectively. The variables g, h_p and D in (**c**) represent the gravitational acceleration, penetration depth and diameter of the projectile, respectively

and H is the distance between the ball release point and the gel surface. Similar pixel measurement was carried out for the penetration depth, which was measured as the initial depth that the projectile could reach when its velocity was equal to zero.

Theory

Cavitation Rheology

The formation of a cavity in a Newtonian liquid can be described by the simple equation $\Delta P = 2\gamma/r$, where ΔP is the pressure difference between the inside and outside of a cavity, γ is the surface tension coefficient of the interface, and r is the radius of the cavity [33]. For the cavity growth in an elastic solid, the pressure is balanced by both surface energy and elastic energy [13]. The restored elastic energy for an incompressible neo-Hookean solid can be characterized by the strain energy density equation $W = \frac{E}{6}(I_1 - 3)$, where E is the Young's modulus, and I_1 is the first invariant of the right Cauchy-Green deformation tensor [34]. The pressure to inflate a cavity is

$$P \cong (\frac{5}{6} - \frac{2}{3\lambda} - \frac{1}{6\lambda^4})E + (\frac{\sqrt{\lambda^2 - 1}}{\lambda^2})(\frac{4\gamma}{r_0}), \tag{1}$$

where λ is the expansion ratio defined as $(A_{sc}/A_0)^{0.5}$ [35–37]. A_{sc} is the surface area of the spherical cap due to the air inflation and A_0 is the cross-sectional area of the needle. r_0 is the inner radius of the needle, representing the size of initial defect. The method to determine the critical expansion ratio λ_c and the corresponding critical pressure P_c at the instability is provided in the "Cavitation Rheology Derivations". In some cavitation rheology experiments, the following equation obtained from curve fitting is applied to determine the Young's modulus and surface tension [36]:

$$P_c^{fit} = \frac{5}{6}E + \frac{2\gamma}{r_0}, \tag{2}$$

It is demonstrated in the "Cavitation Rheology Derivations" that there exists a difference between the critical pressures calculated by equations (1) and (2) for a range of r_0, E and γ values. In view of the difference, equation (1) is used in the analysis.

Static Indentation

For a rigid spherical object indenting a linearly elastic, isotropic and homogeneous half space, the relation between the indentation load F and indentation displacement h is solved by Hertz [38] on the assumption that the contact surface is smooth and that the small deformation is involved. The $F - h$ relation from the Hertzian analysis is

$$F = \frac{4E\sqrt{Rh}h}{3(1 - \nu^2)}, \tag{3}$$

where R is the radius of the indenter, E is Young's modulus and ν is Poisson's ratio. The contact radius α is determined by

$$\alpha = (\frac{3RP(1 - \nu^2)}{4E})^{1/3} \tag{4}$$

Recently, Zhang et al. developed explicit expressions of the F-h relation in the large h/R case based on finite element simulations and dimensional analysis on hyperelastic solids [39]. The newly developed solution could provide accurate results valid up to $h/R = 1$. The F-h relation from their analysis for a neo-Hookean solid is described as

$$F = \frac{16}{3}\mu_0\sqrt{Rh}h(1 - 0.15\frac{h}{R}), \tag{5}$$

where μ_0 is the initial shear modulus of the material. In addition, Sneddon's solution [40] for the F-h relation is applied to verify the results of indentation experiments. The contact radius and Young's modulus can be determined by

$$h = \frac{1}{2}\alpha ln(\frac{R + \alpha}{R - \alpha}) \tag{6}$$

$$F = \frac{E^*}{2}[(\alpha^2 + R^2)ln(\frac{R + \alpha}{R - \alpha}) - 2\alpha R], \tag{7}$$

where E^* is the effective modulus which is defined as

$$\frac{1}{E^*} = \frac{1 - \nu_1^2}{E_1} + \frac{1 - \nu_2^2}{E_2}, \tag{8}$$

where E_1 and ν_1 are Young's modulus and Poisson's ratio of the test material, and E_2 and ν_2 are those of the indenter [41]. Considering the large difference of Young's moduli between the test material (2 − 20 kPa) and the rigid indenter (∼ 200 GPa), equation (8) can be further simplified:

$$\frac{1}{E^*} \approx \frac{1 - \nu_1^2}{E_1} \tag{9}$$

To obtain Young's modulus E, initial shear modulus μ_0 and effective modulus E^*, C_1, C_2 and C_3 are extracted from equations (3), (5), and (7)

$$C_1 = \frac{4\sqrt{Rh}h}{3(1 - \nu^2)} \tag{10}$$

$$C_2 = \frac{16}{3}\sqrt{Rh}h(1 - 0.15\frac{h}{R}) \tag{11}$$

$$C_3 = \frac{1}{2}[(\alpha^2 + R^2)ln(\frac{R+\alpha}{R-\alpha}) - 2\alpha R] \tag{12}$$

When different indenters are applied to the static indentation experiment, the values of C will change correspondingly. With the same test material, there exists a linear relationship between the load F (self-weight of the indenter) and C, and then the required modulus can be estimated from the slope of the trendline in the $F - C$ plot.

Dynamic Low-Velocity Impact

For a solid projectile penetrating into a non-Newtonian fluid (the micellar fluid, for example), Akers and Belmonte altered the Froude number to take elasticity into account [26]. The new elastic Froude number, Fe, can be written as

$$Fe = \frac{\Delta\rho U_0^2}{G}, \tag{13}$$

where $\Delta\rho$ is the density difference between the spherical projectile and the fluid, U_0 is the characteristic velocity at entry, and G is related to the properties of the fluid [26]. The number is the square of Joseph's elastic Mach number [42]. A power-law relationship between the normalized penetration depth h_p/D (D is the diameter of the spherical projectile) and Fe was found, and the corresponding scaling factor was 1/3. In our study, it is assumed that this scaling is also valid for the 4.69% v/v (volume fraction) gel, which has the lowest stiffness among all the test gels. G is considered to be the initial shear modulus of the material (μ_0).

Results and Discussion

Shear Rheology Experiment

The mechanical responses of gel samples obtained from the strain-amplitude sweep experiments are presented in Fig. 2(a) and (b). 7.89% v/v and 11.89% v/v gels exhibit perfect linear elasticity with no deviation, and shear strain fractures occur at 0.75 and 0.54, respectively. Little strain stiffening is observed in the 4.69% v/v gel, which may be due to the fracture-like instability in the network [43]. The relationship between gel's response and sweep frequency is examined in Fig. 2(c). In both small strain ($\gamma = 1\%$) and large strain ($\gamma = 100\%$) cases, the storage moduli (G') of 4.69% v/v increase with the test

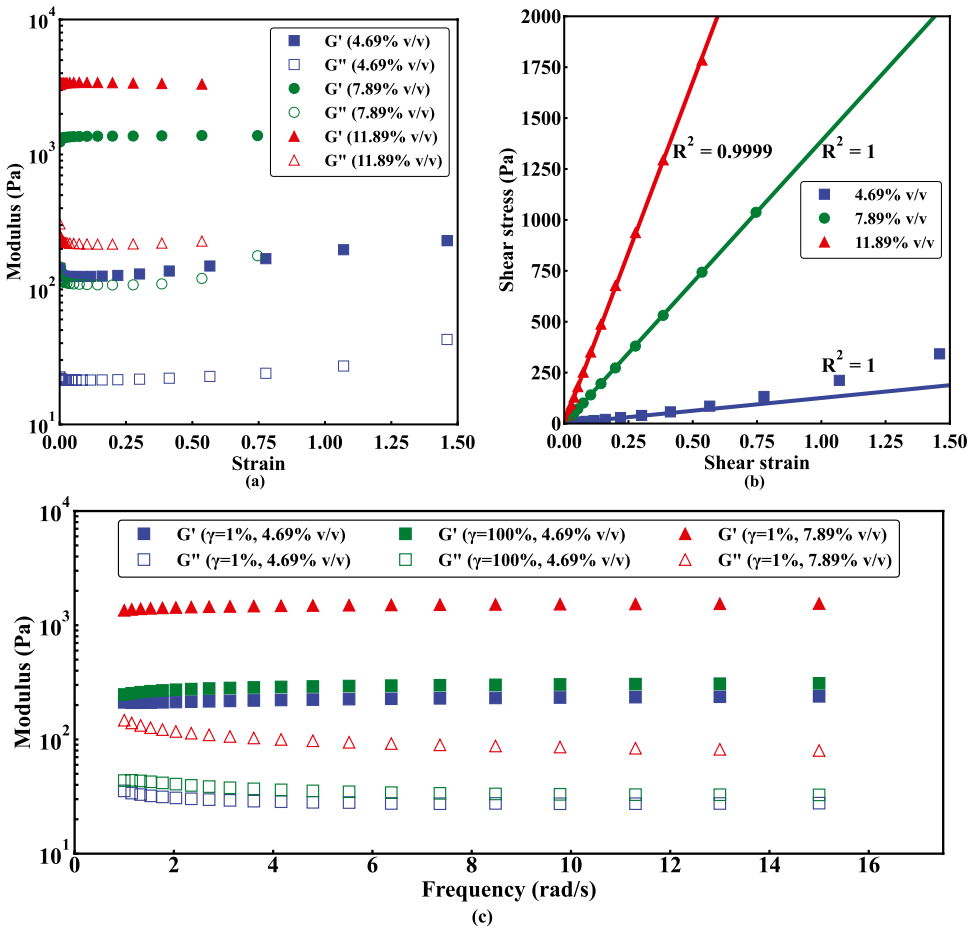

Fig. 2 (**a**) Storage moduli (G') and loss moduli (G'') of three different gels at 1 Hz for various strain amplitudes. (**b**) Stress-strain relationship obtained from the strain-amplitude sweep experiment. (**c**) G' and G'' as a function of frequency for 4.69% v/v (square) and 7.89% v/v (triangle) gels at $\gamma = 1\%$ and $\gamma = 100\%$

frequency. A weaker frequency-dependence on G' is found in 7.89% v/v at $\gamma = 1\%$. G' of 7.89% v/v at $\gamma = 100\%$ is not shown in the same figure due to the occurrence of fracture during a large deformation. In addition, relaxation functions of test materials could be obtained from the storage and loss moduli shown in Fig. 2(c). The results collected from this conversion method are comparable with the values found by shear rheology. Considering the narrow frequency range in the study, a more accurate relaxation behavior of test materials could be extracted from a relaxation experiment over a wide time span.

Cavitation Rheology Experiment

In the cavitation rheology experiment, the measured pressure increases linearly with time and drops at the critical pressure P_c, at which time a rapid unstable expansion occurs. Four needle radii representing different initial defect sizes are involved in the experiment. The parametric study is undertaken for three gel concentrations and an example of the 7.89% v/v gel is illustrated in Fig. 3. The critical pressure P_c for each r_0 can be determined by equation (1) given a set of the Young's modulus E and surface tension γ. Then every single P_c is connected to form a curve. A group of curves generated with different E and γ values are shown in Fig. 3(a) and (b) after narrowing down the range. The parameters that minimize the sum of the errors between the theoretical and experimental critical pressure values are selected to be the Young's modulus and surface tension of the test material. The results of the analysis for different gels are summarized in Table 3. It can be observed that the large r_0 and small r_0 values play a key role in determining the Young's modulus and surface tension, respectively. This is consistent with the previous research work [36]. When the initial defect size decreases, the surface tension has a greater contribution. When the initial defect size increases, the elasticity of the material plays a larger role. The critical pressure P_c is characterized by the balance of surface tension and elasticity.

The radius of the cavity a increases linearly with time in the early stage of the expansion (Fig. 4(a)). The comparison between different needles reflects the fact that a thicker needle generates a faster expansion. The expansion rate of each cavity $\dot{a}$ can be determined by calculating the slope of its corresponding trendline. The von Mises strain rate $\dot{\epsilon}_{vm}$ defined as $\sqrt{\frac{3}{2}\dot{\mathbf{e}}' : \dot{\mathbf{e}}'}$ is introduced to the analysis. Here, $\mathbf{e}$ is the logarithmic finite Hencky strain tensor determined by $\ln\sqrt{F^T F}$ (F is the deformation gradient tensor), and $\mathbf{e}'$ is the deviatoric part of the strain tensor. The von Mises strain rate $\dot{\epsilon}_{vm}$ can be expressed as $2\dot{a}/a$. Notice that the definition of $\dot{\epsilon}_{vm}$ differs from the deformation rate by a factor of 2 in the literature [44]. One example showing $\dot{\epsilon}_{vm}$ of cavity expansion in the 4.69%v/v gel is given in Fig. 4(b).

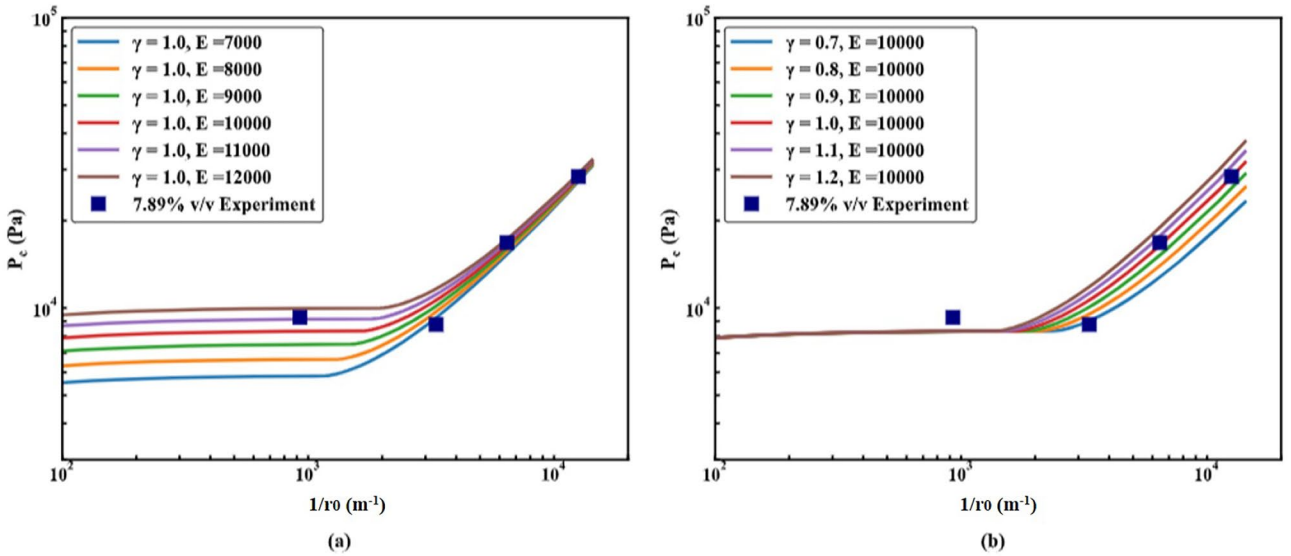

Fig. 3 The parametric study conducted for the 7.89% v/v gel to determine the Young's modulus and surface tension. The unit of Young's modulus is *Pa* and the unit of surface tension is *N/m* in the plot. The blue squares represent the measured critical pressures with four different needles in the cavitation rheology experiment. The value of surface tension is fixed in (**a**), whereas the value of the Young's modulus is fixed in (**b**). Four experiments have been conducted for each applied needle and each gel concentration. The experimental data (solid blue squares) are the calculated average critical pressures

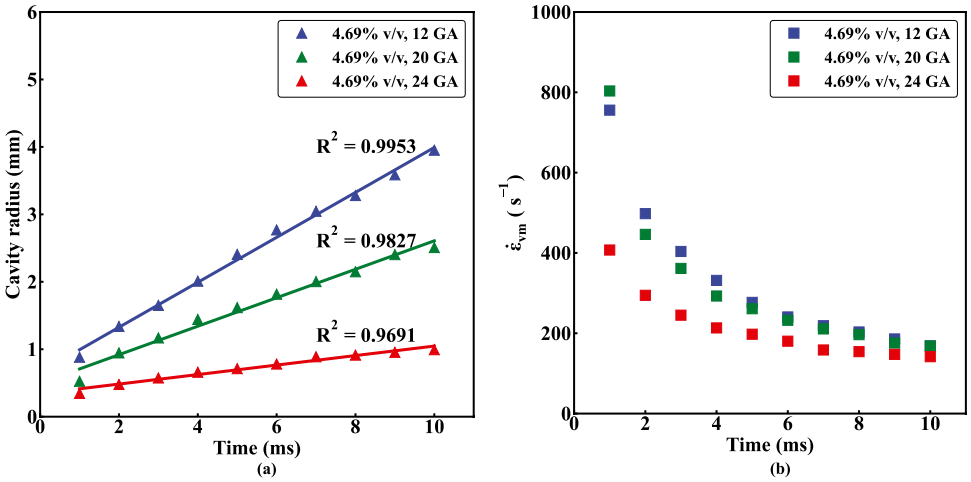

Fig. 4 (**a**) The cavity radius as a function of time during the rapid expansion. (**b**) The von Mises strain rate as a function of time during the same procedure. Three colors represent three different needles in the figures. The gel concentration is 4.69% v/v

Static Indentation Experiment

In the static indentation experiment, both Hertzian and Sneddon's methods were applied to the calculation of contact radius with the measured indentation depth. The comparison between the calculated contact radii and the experimentally measured ones is presented in Fig. 5.

The self-weight F as a function of calculated C_1 (classic Hertzian solution), C_2 (Zhang et al.'s solution) and C_3 (Sneddon's solution) for each indenter are shown in Fig. 6 from (a) to (c). Young's moduli E and initial shear moduli μ_0 of the gels can be determined by estimating the slopes of two trendlines in Fig. 6(a) and (b). On the assumption that the test material is incompressible, the Poisson's ratio ν is 0.5 and Young's modulus E is equal to $3\mu_0$. The effective moduli E^* and the Young's moduli E of two concentrations can be determined using Sneddon's solution according to equations (7) and (9) in the same way (Fig. 6(c)). The non-dimensional plot (Fig. 7) illustrates how the results of Zhang et al. and Sneddon differ from the classic Hertzian theory at large indentation depths. In addition, the contact pressure of each indenter is calculated with the self-weight F and the projected area $\pi\alpha^2$. The linear relationship between the contact pressure and the indenter radius is presented in Fig. 8.

Dynamic Low-Velocity Impact Experiment

The distinctive feature shown in Fig. 9(a), usually referred as pinch-off, is observed in the dynamic low-velocity impact experiment of the 4.69% v/v gel. A funnel shaped temporary cavity above the sphere is formed when the projectile penetrates into the gel. As for the other two concentrations, neither pinch-off nor cavity occurs during the penetration process (Fig. 9(b) and (c)). Akers and Belmonte predicted that the penetration depth would scale with $Fe^{1/3}$ when the cavity forms behind the projectile [26]. On the assumption that this relation is valid in soft gels, the data points from the low-velocity impact experiments should agree well with the data collected from Akers and Belmonte's paper. It can be seen in Fig. 10 that data points representing different projectiles collapse to a single straight line in the log-log plot with the scaling factor close to 1/3. For each projectile, the measured penetration depth h_p is normalized by its diameter D, and the corresponding Fe number can be calculated from the equation of the trendline. With determined h_p/D,

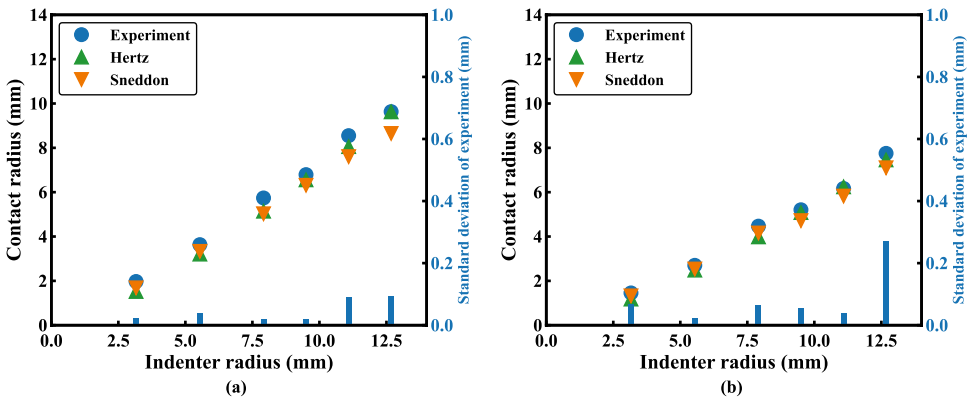

Fig. 5 The comparison between calculated contact radii (using Hertzian and Sneddon's solutions) and the measured contact radii for (**a**) 7.89% v/v and (**b**) 11.89% v/v gels. The standard deviations are marked as blue bars in both plots and the number of measurements taken for each indenter is equal to 4

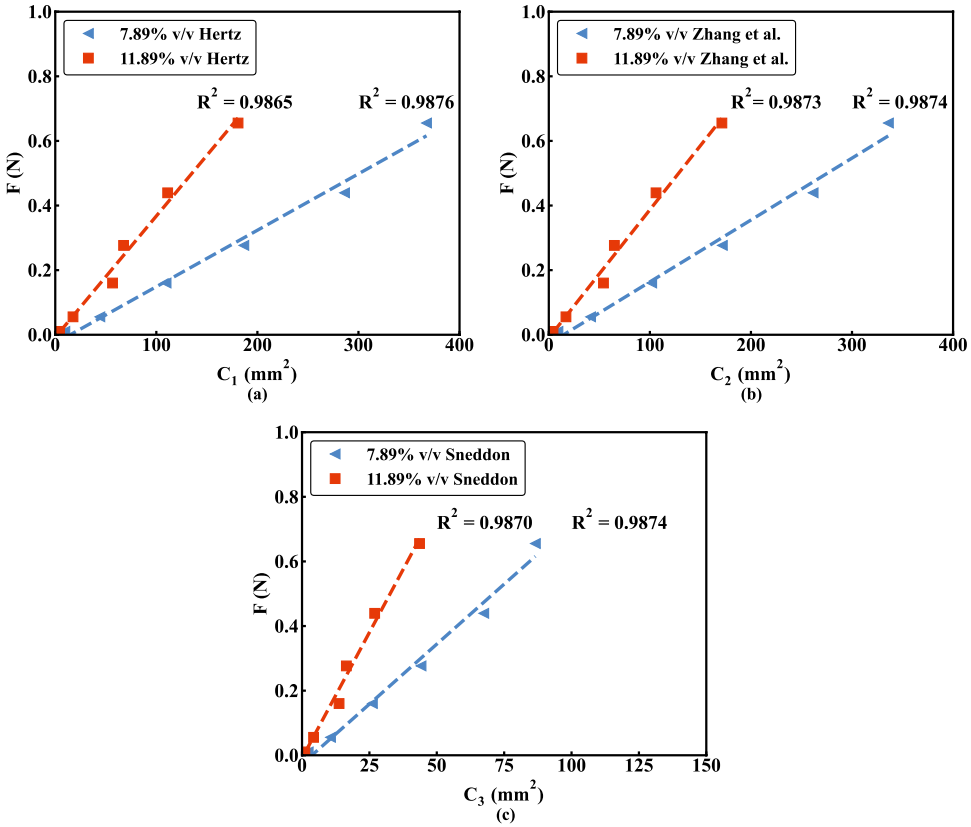

Fig. 6 The load F as a function of C_1, C_2, and C_3 (calculated from equations (10) to (12)) for two different gels. The slopes of trendlines in (**a**), (**b**), and (**c**) reflect Young's moduli E, initial shear moduli μ_0, and effective moduli E^*, respectively

calculated Fe, measured density difference $\Delta\rho$ and impact velocities U_0^2, the initial shear modulus μ_0 of the test gel can be obtained by fitting the low-velocity impact data to the aforementioned trendline according to equation (13).

It is interesting to find that only the 4.69% v/v gel samples can have a reasonable μ_0 value in good agreement with the cavitation rheology experiment. For the other two concentrations, the average value of initial shear modulus is taken between the previous cavitation rheology and static indentation experiments. Each average value is substituted into equation (13) to determine the corresponding Fe. The data points of the higher concentrations in Fig. 10 are located outside the trendline. In terms of the small difference between the results from the cavitation rheology and the low-velocity

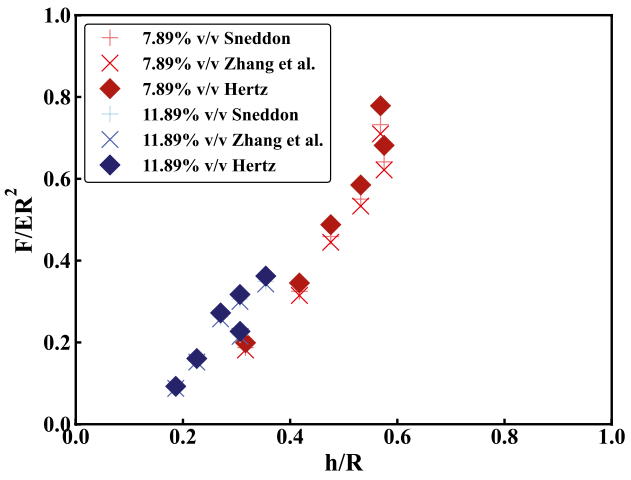

Fig. 7 Non-dimensional plot of the load F-indentation depth h for different indenters and different concentrations. Solutions from Hertzian theory (solid diamonds) are compared with the results of Zhang et al. (cross signs) and Sneddon (plus signs)

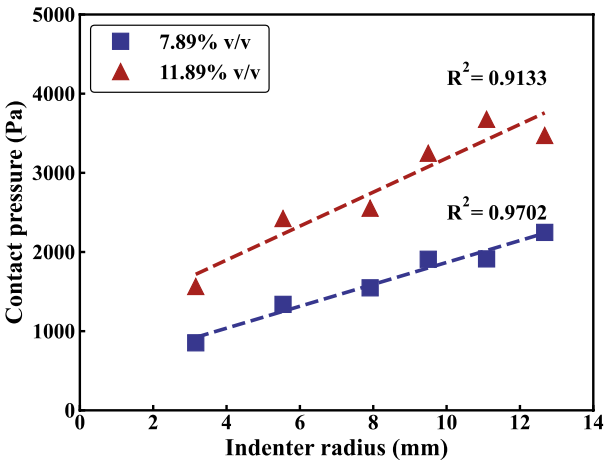

Fig. 8 Contact pressures calculated for different indenters in the indentation experiment

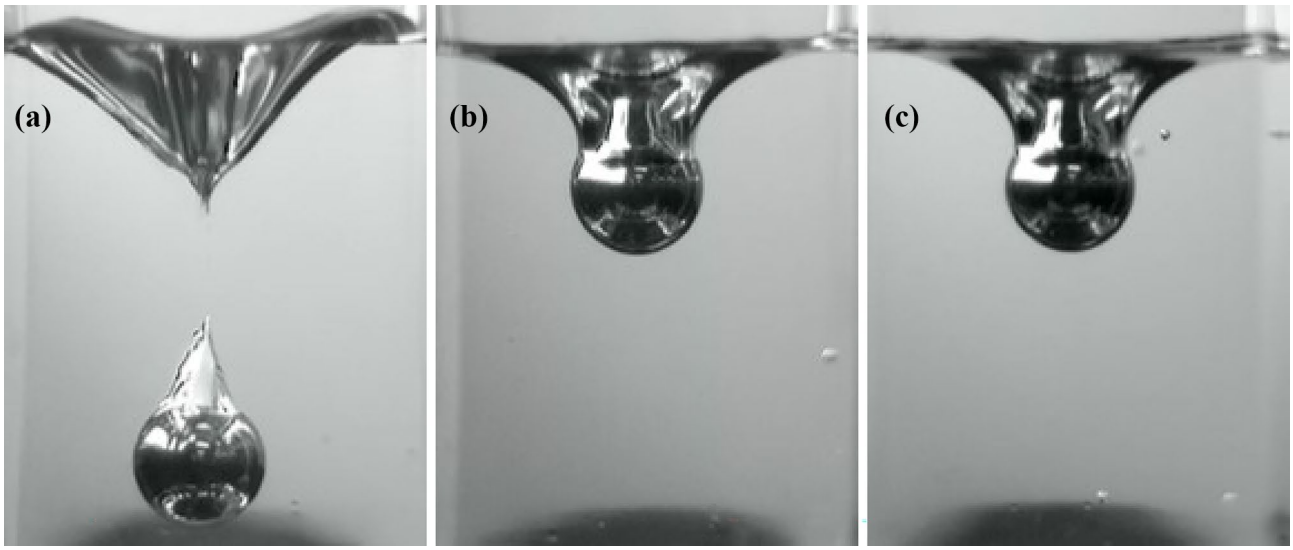

Fig. 9 The images of deepest penetrations in three gels (**a**) 4.69% v/v (**b**) 7.89% v/v (**c**) 11.89% v/v. A clear pinch-off and a cavity formed on the top surface are presented in (**a**). The diameter of the steel ball is 15.79 *mm*

impact experiments for 4.69% v/v gel (Table 3), a conclusion can be drawn that the low-velocity impact method provides a satisfactory solution for determining the Young's modulus of the gel revealing a pinch-off phenomenon under the low-velocity penetration.

The comparison between different experimental methods is summarized in Tables 2 and 3. One advantage of shear rheometry experiments is that the loading conditions (strain, strain rate, and strain state) are known (and controlled) fairly well as a function of time and space. Hence, in Fig. 11 and Table 2 we may precisely report the strain and strain rate at which the storage moduli are measured (as well as approximate associated instantaneous, equilibrium, and relaxation moduli). Unfortunately, the other methods involve complicated stress and strain states that are spatially non-uniform throughout the gel. As such, the interpretation of the associated material property is not straight forward. For example, the derivation of equation (1) utilized to convert the measured cavitation pressure into a material property assumes a rate-independent, incompressible neo-Hookean material. If the material exhibits non-negligible time-dependence then the value of the Young's modulus obtained from equation

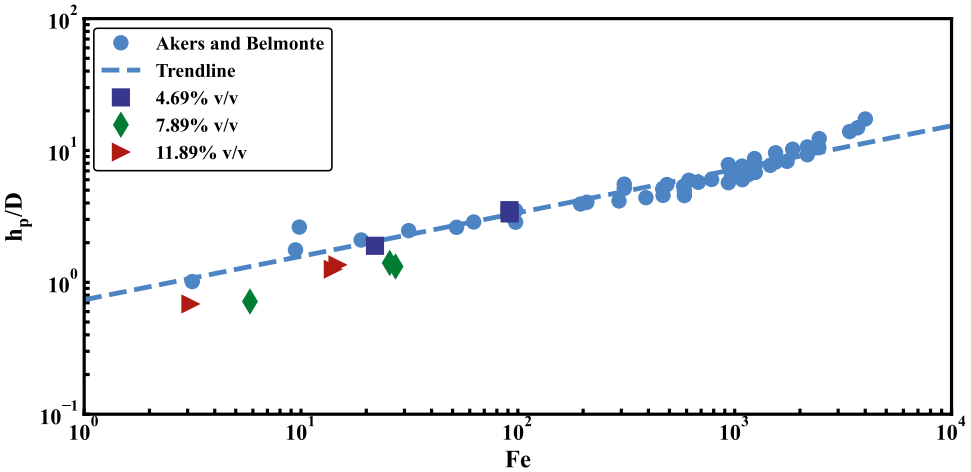

Fig. 10 The data points of 4.69% v/v gel (dark blue squares) fall onto the trendline obtained from Akers and Belmonte's paper (the root-mean-square error is 0.1544 *kPa*), while the other data points fall out of the line with higher error. The data points of 7.89% v/v gel (green diamonds) and 11.89% v/v gel (red triangles) are produced using the average initial shear moduli from cavitation rheology and static indentation experiments. The figure clarifies the limitation of the low-velocity impact method. It is only valid for certain soft materials where a pinch-off phenomenon occurs during the penetration experiment

Table 2 Young's moduli of three gel concentrations measured from the frequency sweep experiments (FS) and strain amplitude sweep experiments (SAS). For the shear rheology experiments, one sample was tested for each gel concentration. N/A, not applicable

	FS at 1 rad/s and $\gamma = 1\%$	FS at 15 rad/s and $\gamma = 1\%$	SAS at 1 Hz
4.69% v/v	0.63	0.72	0.43
7.89% v/v	4.05	4.65	4.17
11.89% v/v	N/A	N/A	10.05

(1) is difficult to interpret. In Fig. 11, we have made an effort to approximate the strain and strain rate that the cavitation experiment is most associated with. It remains to be seen if a shear rheometry test conducted at this strain and strain rate will result in better agreement between the two methods. Similar issues arise in the interpretation of the stiffnesses from the free-fall impact and self-weight induced indentation experiments for which we have similarly approximated their representative strain and strain rates in Fig. 11.

Tables 2 and 3 show that cavitation rheology and low-velocity impact (free-fall impact) experiments produce comparable results, which are larger than the ones from shear rheology and self-weight induced indentation. This noticeable discrepancy can be explained by the difference in the von Mises strain rate $\dot{\epsilon}_{vm}$. For the self-weight induced indentation experiment, the von Mises strain rate calculations are shown in equations (16) to (20) in "Von Mises Strain and Strain Rate Calculation for the Static Indentation Experiment". $\dot{\epsilon}_{vm}$ can be calculated by $2\dot{h}/h$, where $\dot{h}$ is the indentation speed and h is the indentation depth. For a free-fall impact experiment, $\dot{\epsilon}_{vm}$ is determined by $4U_0/(2h_p + D)$, where U_0 is the impact velocity, h_p is the penetration depth, and D is the diameter of the projectile. The detailed calculations and derivations can be found from equations (21) to (27) in "Von Mises Strain and Strain Rate Calculation for the Free-Fall Impact Experiment". Notice that the bounds of mentioned experiments shown in Fig. 11 are only for the specific gel sample and the particular experiment settings, which cannot represent the limits of general experiments. Different stress states are examined in the gel characterization procedure: tension (cavitation), compression (indentation and free-fall impact), and shear (shear rheology). Here, the test materials during indentation and impact experiments are considered to be under

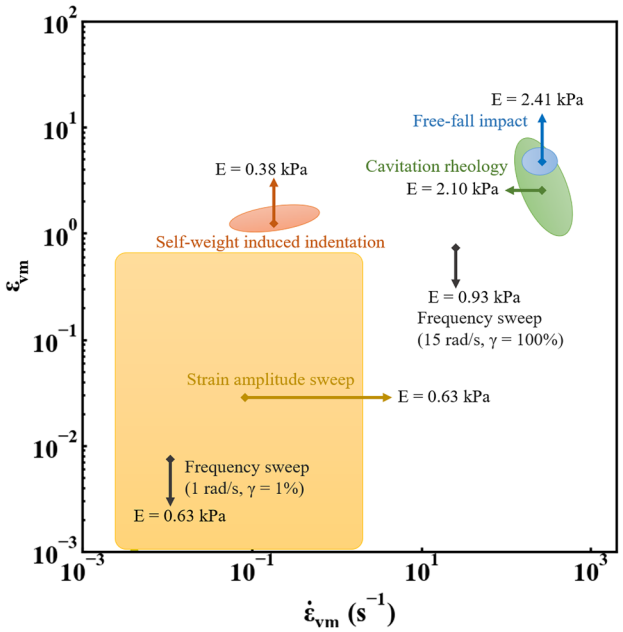

Fig. 11 Diagram of the von Mises strain against the von Mises strain rate for four different experimental methods: strain-amplitude-sweep shear rheology at 1 Hz (yellow), frequency sweep experiment at 1 rad/s and $\gamma = 1\%$ and at 15 rad/s and $\gamma = 100\%$ (grey), self-weight induced indentation (orange), cavitation rheology with 12 GA needle (green), and free-fall impact test (blue). The concentration of the gel sample in this diagram is 4.69 % v/v. The Young's moduli predicted by different experiments are also included. The areas of the ovals are estimated for different experimental methods based on the collected experimental data

compression since only the edge of the contact region experiences tension. It appears that $\dot{\epsilon}_{vm}$ of both cavitation rheology and free-fall impact experiments are of the same order of magnitude, which are higher than those in shear rheology and indentation methods (Fig. 11). These results show a slight strain-rate dependence in gel stiffness, which agrees with previous literature in similar polymers [30, 45–47]. Another possible reason for the variance in the gel stiffness between these experiments is that non-reversible cavities or fractures could be generated during a cavitation rheology experiment. This can affect the measurement of critical pressure. It is an ongoing challenge to distinguish cavitation and fracture. Further research needs to be done to better understand the relationship between cavitation and fracture.

Table 3 Young's moduli of three gel concentrations measured from cavitation rheology, static indentation and dynamic low-velocity impact experiments. The unit of the experimental data is kPa, and the standard deviations are included. N/A, not applicable

	Cavitation	Indentation Zhang et al.	Indentation Sneddon	Low-velocity impact
4.69% v/v	2.10	0.38 ± 0.01	0.37 ± 0.01	2.41 ± 0.57
7.89% v/v	11.00	5.75 ± 0.32	5.57 ± 0.31	N/A
11.89% v/v	19.00	11.90 ± 0.68	11.68 ± 0.67	N/A

Conclusion

This study provides a comprehensive analysis of pragmatic stiffness measurement techniques (cavitation rheology, static indentation and dynamic low-velocity impact) for measuring linear elastic properties of bulk gel, and demonstrates their usefulness across various stiffness regimes. This study underscores the importance in selecting the proper experimental method based on inherent limitations and strain rates of interest. One major limitation of these experimental methods is that the test gel has to be transparent for optical measurements. Although this study shows a slight strain-rate dependence in the particular gel of interest, it is important to note that different gel types might exhibit a larger strain rate dependence, or a larger strain stiffening response.

When seeking linear elastic properties for bulk measurements of gels, cavitation rheology (a relatively new technique) showed reliable results that are comparable with conventional experimental techniques. The comparison between different experimental methods with conventional benchmark testing (parallel plate rheology) indicates that cavitation rheology is correlated with material properties obtained in high-strain rate experiments. The results of cavitation rheology were significantly different from quasi-static test results. For the same gel material, the higher strain-rate experiments such as cavitation rheology and low-velocity impact will lead to higher Young's moduli compared with those obtained from shear rheology and static indentation. The dynamic low-velocity impact experiment gives a similar result to cavitation rheology for the softest material (4.69% v/v); however, this technique requires that the gel is soft enough so that a pinch-off occurs.

These results collectively suggest that cavitation rheology, as well as the other simplistic experimental techniques examined in this study, can become useful, inexpensive, and accurate tools in the characterization of complex soft materials.

Appendix

Cavitation Rheology Derivations

The critical expansion ratio at the instability λ_c can be determined by setting the derivative of equation (1) with respect to λ equal to zero

$$\frac{4}{Er_0}\left(\frac{-2\gamma\sqrt{\lambda_c^2-1}}{\lambda_c^3}+\frac{\gamma}{\lambda_c\sqrt{\lambda_c^2-1}}\right)+\frac{2}{3}\left(\frac{1}{\lambda_c^2}+\frac{1}{\lambda_c^5}\right)=0, \quad (14)$$

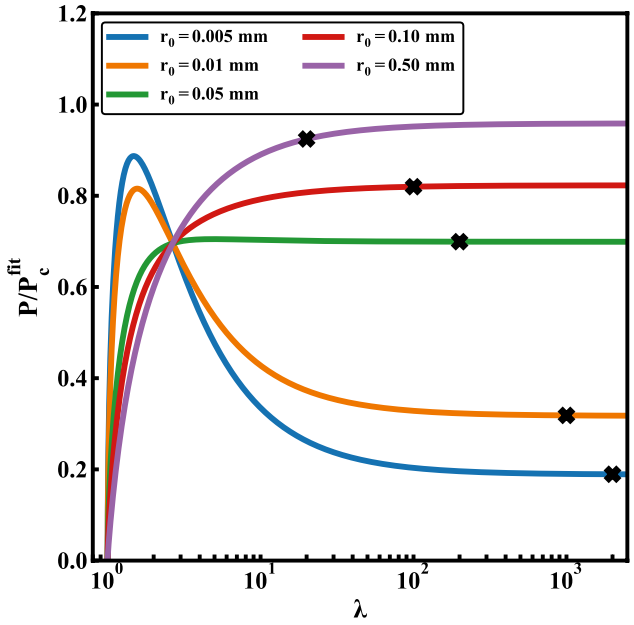

Fig. 12 E and γ are assumed as 3 kPa and 0.0269 N/m for the plot. P is calculated by equation (1), and P_c^{fit} is calculated by equation (2). For a small r_0 value (0.005 mm and 0.01 mm), the pressure ratio P/P_c^{fit} reaches a maximum and then decreases with the increase of expansion ratio λ. For a large r_0 value (0.05 mm, 0.10 mm and 0.50 mm), P/P_c^{fit} monotonically increases and asymptotically approaches a certain value. The maximum of P/P_c^{fit} is not equal to 1 for some r_0 values, reflecting the difference in maximum pressures (critical pressures) calculated by equations (1) and (2). The black cross (x) on each curve demonstrates the expansion ratio at which the cavity reaches the inner surface of the gel container, assuming the inner radius of the container to be 10 mm

The critical pressure at the instability P_c is calculated by substituting λ_c for λ in equation (1)

$$P_c \cong \left(\frac{5}{6}-\frac{2}{3\lambda_c}-\frac{1}{6\lambda_c^4}\right)E+\left(\frac{\sqrt{\lambda_c^2-1}}{\lambda_c^2}\right)\left(\frac{4\gamma}{r_0}\right), \quad (15)$$

The difference between the critical pressures calculated by equations (1) and (2) is illustrated in Fig. 12. One example of linear regression based on equation (2) is presented in Fig. 13.

Von Mises Strain and Strain Rate Calculation for the Static Indentation Experiment

The calculations of von Mises strain and strain rate for the static indentation experiment are as follows: The deformation gradient tensor $\mathbf{F}$ can be expressed as

$$\begin{bmatrix} \sqrt{\frac{A_s}{A_c}} & 0 & 0 \\ 0 & \sqrt{\frac{A_s}{A_c}} & 0 \\ 0 & 0 & \frac{A_c}{A_s} \end{bmatrix} \quad (16)$$

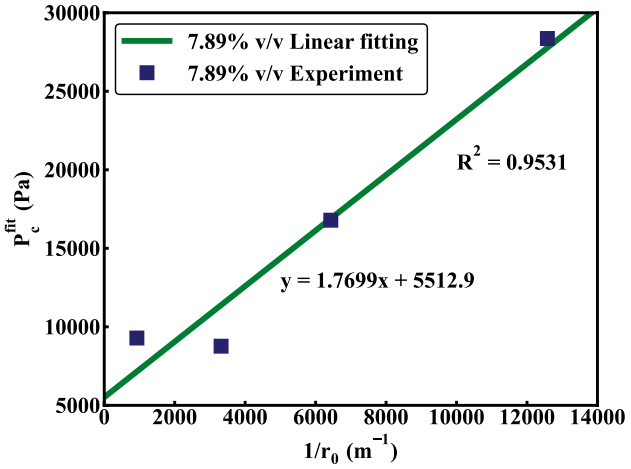

Fig. 13 An example of linear regression performed for our 7.89% v/v gel using equation (2). E and γ are calculated to be 6.6 kPa and 0.88 N/m in this case

where A_s and A_c are the surface area of the spherical cap which is surrounded by gel and the contact area (projected area), respectively. The ratio between A_s and A_c can be expressed as

$$\frac{A_s}{A_c} = \frac{2Rh}{\alpha^2} \tag{17}$$

where R is the radius of indenter, h is the indentation depth and α is the contact radius. The logarithmic finite Hencky strain tensor $\mathbf{e}$ is

$$\mathbf{e} = \ln\sqrt{\mathbf{F}^{\mathrm{T}}\mathbf{F}} = \begin{bmatrix} \ln\left(\frac{A_s}{A_c}\right) & 0 & 0 \\ 0 & \ln\left(\frac{A_s}{A_c}\right) & 0 \\ 0 & 0 & 2\ln\left(\frac{A_c}{A_s}\right) \end{bmatrix} \tag{18}$$

The von Mises strain $\varepsilon_{\mathrm{vm}}$ can then be calculated with the deviatoric part of the logarithmic finite Hencky strain tensor $\mathbf{e}'$

$$\varepsilon_{\mathrm{vm}} = \sqrt{\frac{2}{3}\mathbf{e}' : \mathbf{e}'} = \frac{2Rh}{\alpha^2} \tag{19}$$

We take the derivative of equation (18) with respect to time, we can calculate the von Mises strain rate $\dot{\varepsilon}_{\mathrm{vm}}$ is determined

$$\dot{\varepsilon}_{\mathrm{vm}} = \sqrt{\frac{2}{3}\dot{\mathbf{e}}' : \dot{\mathbf{e}}'} = 2\frac{\dot{h}}{h} \tag{20}$$

where $\dot{h}$ is the indentation speed, which is estimated by $\sqrt{2gh}$ and h is the indentation depth.

Von Mises Strain and Strain Rate Calculation for the Free-Fall Impact Experiment

The calculations of von Mises strain and strain rate for the free-fall impact experiment are as follows: The deformation gradient tensor $\mathbf{F}$ can be expressed as

$$\begin{bmatrix} \sqrt{\frac{A_s}{A_c}} & 0 & 0 \\ 0 & \sqrt{\frac{A_s}{A_c}} & 0 \\ 0 & 0 & \frac{A_c}{A_s} \end{bmatrix} \tag{21}$$

where A_s and A_c are the estimated surface area of a cylinder created during the penetration process and the contact area (projected area), respectively. A_s and A_c can be calculated by

$$A_s = \pi D h_p + \frac{\pi D^2}{2} \tag{22}$$

$$A_c = \frac{\pi D^2}{4} \tag{23}$$

The ratio between A_s and A_c can be expressed as

$$\frac{A_s}{A_c} = 2 + 4\frac{h_p}{D} \tag{24}$$

where h_p is the penetration depth, D is the diameter of the projectile. The logarithmic finite Hencky strain tensor $\mathbf{e}$ is

$$\mathbf{e} = \ln\sqrt{\mathbf{F}^{\mathrm{T}}\mathbf{F}} = \begin{bmatrix} \ln\left(\frac{A_s}{A_c}\right) & 0 & 0 \\ 0 & \ln\left(\frac{A_s}{A_c}\right) & 0 \\ 0 & 0 & 2\ln\left(\frac{A_c}{A_s}\right) \end{bmatrix} \tag{25}$$

The von Mises strain $\varepsilon_{\mathrm{vm}}$ can then be calculated with the deviatoric part of the logarithmic finite Hencky strain tensor $\mathbf{e}'$

$$\varepsilon_{\mathrm{vm}} = \sqrt{\frac{2}{3}\mathbf{e}' : \mathbf{e}'} = 2\ln\left(2 + 4\frac{h_p}{D}\right) \tag{26}$$

We take the derivative of equation (25) with respect to time, we can calculate the von Mises strain rate $\dot{\varepsilon}_{\mathrm{vm}}$ is determined

$$\dot{\varepsilon}_{\mathrm{vm}} = \sqrt{\frac{2}{3}\dot{\mathbf{e}}' : \dot{\mathbf{e}}'} = \frac{4U_0}{2h_p + D} \tag{27}$$

where U_0 is the impact velocity.

Supplementary Plots for Static Indentation Experiment with 4.69% v/v Gel

See Figs. 14, 15, and 16.

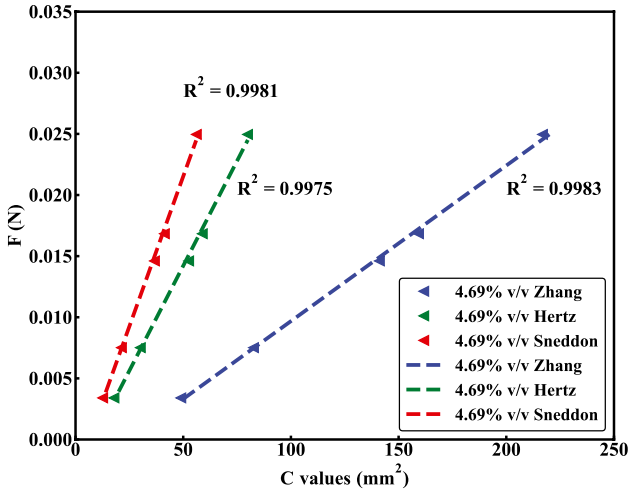

Fig. 14 The load F as a function of C values (C_1, C_2, and C_3) calculated from equations (10) to (12) for the 4.69% v/v gel sample. The dashed trendlines are also included in the plot

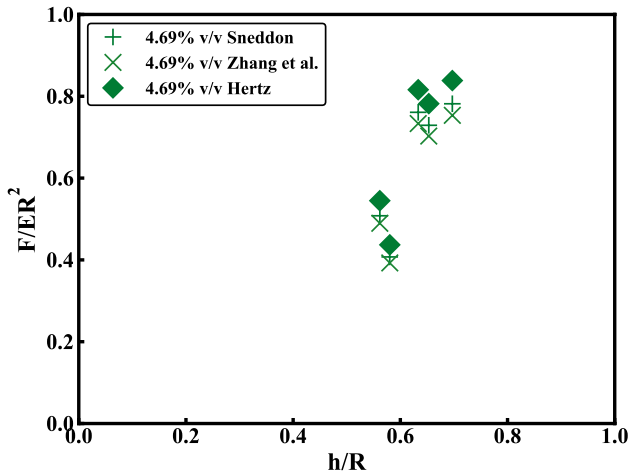

Fig. 15 Non-dimensional plot of the load F-indentation depth h for different indenters of 4.69% v/v gel sample. Solutions from Hertzian theory (solid diamonds) are compared with the results of Zhang et al. (cross signs) and Sneddon (plus signs)

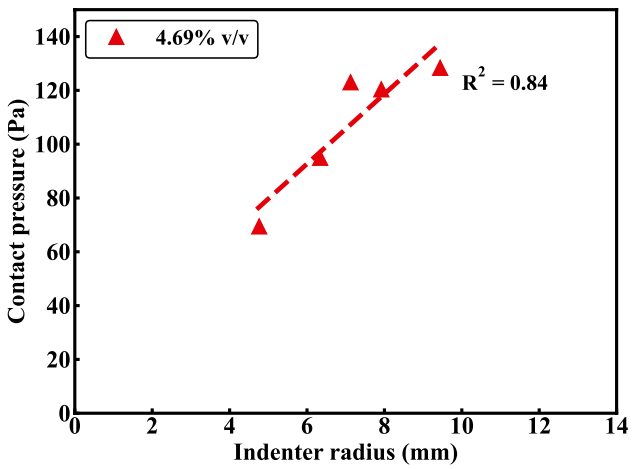

Fig. 16 Contact pressures calculated for different hollow aluminum indenters in the indentation experiment of 4.69% v/v gel sample

Acknowledgements Portions of this research were sponsored by the ASME Haythornthwaite Foundation Research Initiation Grant as well as the Army Research Laboratory under Cooperative Agreement Number W911NF-12-2-0022. The views and conclusions contained in this document are those of the authors and should not be interpreted as representing the official policies, either expressed or implied, of the Army Research Laboratory or the U.S. Government. The U.S. Government is authorized to reproduce and distribute reprints for Government purposes notwithstanding any copyright notation herein. We also thank Prof. Chandler Benjamin and Alexandria Trevino for the assistance with shear rheology experiments.

Declarations

Conflicts of Interest The authors declare that they have no conflict of interest.

References

1. Ferry JD (1980) Viscoelastic properties of polymers. John Wiley & Sons
2. Kononov S, Brewer K, Sakai H, Cavalcante FS, Sabayanagam CR, Ingenito EP, Suki B (2001) Roles of mechanical forces and collagen failure in the development of elastase-induced emphysema. Am J Respir Crit Care Med 164(10):1920–1926
3. Liu F, Mih JD, Shea BS, Kho AT, Sharif AS, Tager AM, Tschumperlin DJ (2010) Feedback amplification of fibrosis through matrix stiffening and cox-2 suppression. J Cell Biol 190(4):693–706
4. Yuan H, Kononov S, Cavalcante FS, Lutchen KR, Ingenito EP, Suki B (2000) Effects of collagenase and elastase on the mechanical properties of lung tissue strips. J Appl Physiol 89(1):3–14
5. Sherratt MJ (2009) Tissue elasticity and the ageing elastic fibre. Age 31(4):305–325
6. Angelova N, Hunkeler D (1999) Rationalizing the design of polymeric biomaterials. Trends Biotechnol 17(10):409–421
7. Balgude A, Yu X, Szymanski A, Bellamkonda R (2001) Agarose gel stiffness determines rate of DRG neurite extension in 3D cultures. Biomaterials 22(10):1077–1084
8. Lutolf MP, Gilbert PM, Blau HM (2009) Designing materials to direct stem-cell fate. Nature 462(7272):433–441
9. Yeh WC, Li PC, Jeng YM, Hsu HC, Kuo PL, Li ML, Yang PM, Lee PH (2002) Elastic modulus measurements of human liver and correlation with pathology. Ultrasound Med Biol 28(4):467–474
10. Lyshchik A, Higashi T, Asato R, Tanaka S, Ito J, Hiraoka M, Brill A, Saga T, Togashi K (2005) Elastic moduli of thyroid tissues under compression. Ultrason Imaging 27(2):101–110
11. Liu K, VanLandingham MR, Ovaert TC (2009) Mechanical characterization of soft viscoelastic gels via indentation and optimization-based inverse finite element analysis. J Mech Behav Biomed Mater 2(4):355–363
12. Han CS, Sanei SH, Alisafaei F (2016) On the origin of indentation size effects and depth dependent mechanical properties of elastic polymers. J Polym Eng 36(1):103–111
13. Zimberlin JA, Sanabria-DeLong N, Tew GN, Crosby AJ (2007) Cavitation rheology for soft materials. Soft Matter 3(6):763–767
14. Fuentes-Caparrós AM, Dietrich B, Thomson L, Chauveau C, Adams DJ (2019) Using cavitation rheology to understand dipeptide-based low molecular weight gels. Soft Matter 15(31):6340–6347
15. Hashemnejad SM, Kundu S (2019) Rheological properties and failure of alginate hydrogels with ionic and covalent crosslinks. Soft Matter 15(39):7852–7862

16. Jansen LE, Birch NP, Schiffman JD, Crosby AJ, Peyton SR (2015) Mechanics of intact bone marrow. J Mech Behav Biomed Mater 50:299–307
17. Pavlovsky L, Ganesan M, Younger JG, Solomon MJ (2014) Elasticity of microscale volumes of viscoelastic soft matter by cavitation rheometry. Appl Phys Lett 105(11):114105
18. Doperalski AE, Tester NJ, Jefferson SC, Howland DR (2011) Altered obstacle negotiation after low thoracic hemisection in the cat. J Neurotrauma 28(9):1983–1993
19. Elder GA, Mitsis EM, Ahlers ST, Cristian A (2010) Blast-induced mild traumatic brain injury. Psychiatr Clin 33(4):757–781
20. Kurosawa Y, Kato K, Saito S, Kubo M, Uzuka T, Fujii Y, Takahashi H (2009) Basic study of brain injury mechanism caused by cavitation. In: 2009 Annual International Conference of the IEEE Engineering in Medicine and Biology Society. IEEE, pp 7224–7227
21. Salzar RS, Treichler D, Wardlaw A, Weiss G, Goeller J (2017) Experimental investigation of cavitation as a possible damage mechanism in blast-induced traumatic brain injury in post-mortem human subject heads. J Neurotrauma 34(8):1589–1602
22. Birkhoff G et al (2012) Jets, wakes, and cavities, vol 2. Elsevier
23. Gaudet S (1998) Numerical simulation of circular disks entering the free surface of a fluid. Phys Fluids 10(10):2489–2499
24. Glasheen J, McMahon T (1996) Vertical water entry of disks at low froude numbers. Phys Fluids 8(8):2078–2083
25. Richardson E (1948) The impact of a solid on a liquid surface. Proc Phys Soc 61(4):352
26. Akers B, Belmonte A (2006) Impact dynamics of a solid sphere falling into a viscoelastic micellar fluid. J Non-Newtonian Fluid Mech 135(2–3):97–108
27. Mrozek RA, Leighliter B, Gold CS, Beringer IR, Jian HY, VanLandingham MR, Moy P, Foster MH, Lenhart JL (2015) The relationship between mechanical properties and ballistic penetration depth in a viscoelastic gel. J Mech Behav Biomed Mater 44:109–120
28. Seitz ME, Burghardt WR, Faber K, Shull KR (2007) Self-assembly and stress relaxation in acrylic triblock copolymer gels. Macromolecules 40(4):1218–1226
29. Erk KA, Henderson KJ, Shull KR (2010) Strain stiffening in synthetic and biopolymer networks. Biomacromolecules 11(5):1358–1363
30. Kundu S, Hashemnejad SM, Zabet M, Mishra S (2018) Self-assembly and mechanical properties of a triblock copolymer gel in a mid-block selective solvent. In: Gels and Other Soft Amorphous Solids. ACS Publications, pp 157–197
31. Drzal PL, Shull KR (2003) Origins of mechanical strength and elasticity in thermally reversible, acrylic triblock copolymer gels. Macromolecules 36(6):2000–2008
32. Hashemnejad SM, Kundu S (2015) Nonlinear elasticity and cavitation of a triblock copolymer gel. Soft Matter 11(21):4315–4325
33. Young T (1805) III an essay on the cohesion of fluids. Phil Trans R Soc London 95:65–87
34. Ogden RW (1997) Non-linear elastic deformations. Courier Corporation
35. Gent A (2005) Elastic instabilities in rubber. Int J Non Linear Mech 40(2–3):165–175
36. Kundu S, Crosby AJ (2009) Cavitation and fracture behavior of polyacrylamide hydrogels. Soft Matter 5(20):3963–3968
37. Lin YY, Hui CY (2004) Cavity growth from crack-like defects in soft materials. Int J Fract 126(3):205–221
38. Hertz H (1882) Ueber die berührung fester elastischer körper. J Reine Angew Math 1882(92):156–171
39. Zhang MG, Cao YP, Li GY, Feng XQ (2014) Spherical indentation method for determining the constitutive parameters of hyperelastic soft materials. Biomech Model Mechanobiol 13(1):1–11
40. Sneddon IN (1965) The relation between load and penetration in the axisymmetric boussinesq problem for a punch of arbitrary profile. Int J Eng Sci 3(1):47–57
41. Stilwell N, Tabor D (1961) Elastic recovery of conical indentations. Proc Phys Soc 78(2):169
42. Ramos J (1991) DD Joseph, Fluid dynamics of viscoelastic liquids. Springer-Verlag, New York (1990)
43. Berret JF, Séréro Y (2001) Evidence of shear-induced fluid fracture in telechelic polymer networks. Phys Rev Lett 87(4):048303
44. Delbos A, Cui J, Fakhouri S, Crosby AJ (2012) Cavity growth in a triblock copolymer polymer gel. Soft Matter 8(31):8204–8208
45. Cuvelier G, Launay B (1990) Frequency dependence of viscoelastic properties of some physical gels near the gel point. In: Makromolekulare Chemie. Macromolecular Symposia, vol 40. Wiley Online Library, pp 23–31
46. Mahaffy R, Shih C, MacKintosh F, Käs J (2000) Scanning probe-based frequency-dependent microrheology of polymer gels and biological cells. Phys Rev Lett 85(4):880
47. Ponton A, Warlus S, Griesmar P (2002) Rheological study of the sol-gel transition in silica alkoxides. J Colloid Interface Sci 249(1):209–216